Distance-of-Flight Mass Spectrometry: A New Paradigm for Mass Separation and Detection

Christie G. Enke,[1] Steven J. Ray,[2] Alexander W. Graham,[2] Elise A. Dennis,[2] Gary M. Hieftje,[2] Anthony J. Carado,[3] Charles J. Barinaga,[3] and David W. Koppenaal[3]

[1]Department of Chemistry, University of New Mexico, Albuquerque, New Mexico 87131-1096; email: enke@unm.edu

[2]Department of Chemistry, Indiana University, Bloomington, Indiana 47405; email: sjray@indiana.edu, alexgrah@indiana.edu, eadennis@umail.iu.edu, hieftje@indiana.edu

[3]Pacific Northwest National Laboratory, Richland, Washington 99352; email: anthony.carado@pnl.gov, charles.barinaga@pnl.gov, david.koppenaal@pnl.gov

Annu. Rev. Anal. Chem. 2012. 5:487–504

First published online as a Review in Advance on April 9, 2012

The *Annual Review of Analytical Chemistry* is online at anchem.annualreviews.org

This article's doi: 10.1146/annurev-anchem-091411-121050

1936-1327/12/0719-0487$20.00

Keywords

array detection, dynamic range, simultaneous analysis, ion focusing, mass analysis

Abstract

Distance-of-flight mass spectrometry (DOFMS) offers the advantages of physical separation of ions, array detection of ions, focusing of initial ion energy, great simplicity, and a truly unlimited mass range. DOFMS instrumentation is similar to that of time-of-flight mass spectrometry (TOFMS) and shares its ion-source versatility, batch analysis, and rapid spectral-generation rate. With constant-momentum ion acceleration and an ion mirror, there is a time at which ions of all mass-to-charge values are energy focused at their particular distances along the flight path. A pulsed field orthogonal to the flight path drives the ions to reach the detector array at this specific time. Results from a 0.29-m proof-of-principle instrument verify the theoretically predicted energy focus and demonstrate how the range of mass-to-charge values that impinge on the detector array can be readily changed. DOFMS could be combined sequentially with TOFMS to enable simultaneous scanless tandem mass spectrometry.

1. INTRODUCTION

Distance-of-flight mass spectrometry (DOFMS), like time-of-flight mass spectrometry (TOFMS), exploits the fact that ions subject to the same impetus have velocities that depend on the mass-to-charge ratio (*m/z*) of the ions; ions with lower *m/z* values have higher velocities. Traveling along a collision-free, field-free flight path, they spatially separate, with lower *m/z* ions taking the lead. In TOFMS, ions are detected at the end of the flight path, appearing in order of increasing *m/z* values. A simple relationship relates arrival time to *m/z*, so a mass spectrum is readily obtained by plotting the ion flux versus arrival time (converted to its equivalent *m/z*). Such velocity-based separation is similar to that obtained in column chromatography, or in a 100-m footrace, in which the distance of the path followed by all the analytes, or runners, is a constant. In an alternative form of separation based on velocity differences, one measures how far each analyte species (or runner) moves in a given length of time. Measuring distance traveled (after a fixed time period) is the basis of thin-layer chromatography, but until now, this method of separation has not been applied in mass spectrometry.

1.1. Overview

Figure 1 depicts a hypothetical DOFMS instrument (1). Ions in a segment of the initial ion beam are accelerated into an ion mirror, whence they exit into a field-free flight path parallel to the plane of an ion detector array. At a set time after their acceleration, all of the ions are then orthogonally pulsed toward a detector array. Because the ions have spread out along the flight path according to their *m/z* values, the more distant detector elements detect the smaller-*m/z* ions, and the ions with larger *m/z* values land on the nearer detector elements. Even though both TOFMS and DOFMS instruments depend on the principle of velocity-based separation and consist of many of the same physical components, their methods of operation and detection are very different. In

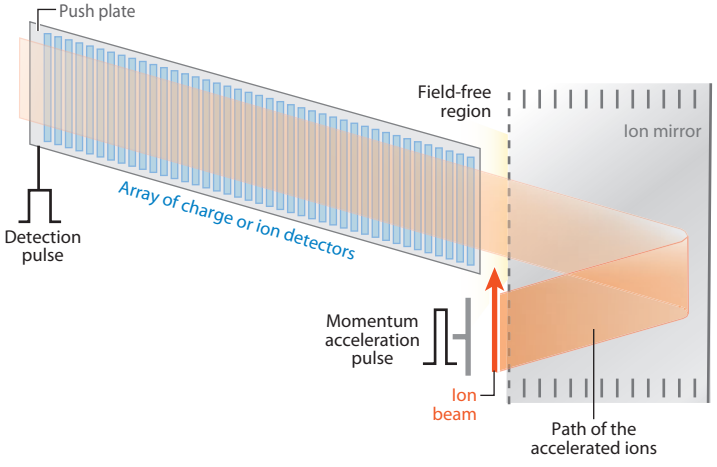

Figure 1

Ions in segments of the initial ion beam are orthogonally accelerated into an ion mirror. In the field-free region past the mirror exit, ions separate according to their velocities; ions with the lowest *m/z* have the leading positions. At the detection time, the entire set of dispersed ions is driven to an array of detectors located parallel to the flight path. The detector elements closer to the mirror detect the ions with the largest *m/z*. After one or more segments of the ion beam have been extracted, the accumulated charge or response on each detector element is read out. From the element positions and intensities, a mass spectrum is produced.

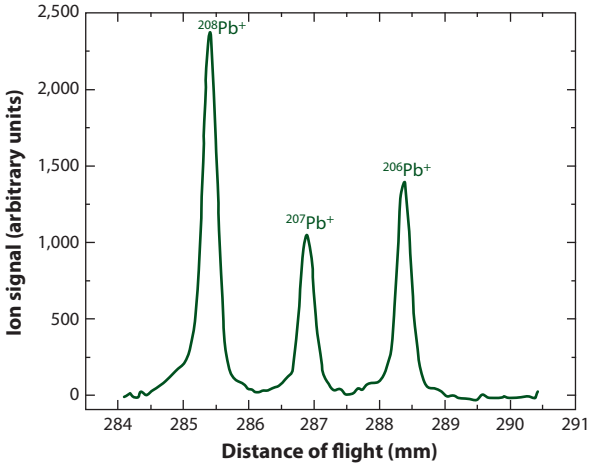

Figure 2

A plot of signal–versus–detector element position in a distance-of-flight mass spectrometer. The three isotopic masses of lead are baseline separated, which indicates complete physical separation and independent detection of each isotope. Reproduced from Reference 2 with permission.

TOFMS, arrival time is related to *m/z*. In DOFMS, an ion's *m/z* value is derived from the location of the detector element upon which the ion lands. In TOFMS, a single detector (or parallel set of detectors) detects all the ions, producing a transient signal that must be interpreted as to ion flux at each arrival time by high-speed electronics. In DOFMS, the various elements of the array detector act independently, and detection is not time related. When the signal level at each element of the array is recorded, the element position is related to *m/z*, and the accumulated signal is proportional to the ion abundance at that *m/z* value.

Figure 2 shows an example of a DOFMS spectrum (2). This spectrum was obtained using a proof-of-principle instrument constructed in the Hieftje lab; it is described in Section 3 of this review. A mass resolving power of 1,000 was obtained in an instrument with a field-free flight path length of only 29.0 cm.

Many of the advantages of DOFMS over existing methods of mass analysis arise from its inherent compatibility with array detection. Array detection spreads the very large information load of the rapidly generated spectra over many detector elements instead of only one, which reduces band-pass requirements and increases achievable dynamic range. Signals from multiple ion extractions can accumulate on the detectors, thereby improving signal-to-noise ratios and further reducing the required flux of data. Additional advantages of DOFMS arise from the method used to focus isobaric (same-*m/z*) ions at each detector. In DOFMS, the focus of ions with initial dispersions of energy and location is complementary to that used in TOFMS and offers the potential for very high resolution in certain situations.

1.2. History and Progress

The concept of distance of flight was first described by Enke (3) in U.S. patent 7,041,968, titled "Distance-of-flight spectrometer for MS and simultaneous scanless MS/MS." This patent illustrates that all the ionic products of all the precursor ions can be simultaneously detected without losing the information about which precursor *m/z* produced each product ion. The precursor's *m/z* information is encoded in the distance of flight while the product *m/z* is obtained by TOFMS (this

potential application of DOFMS is described in more detail in Section 4.5). Before this technique could be incorporated into a tandem mass spectrometer, some fundamental aspects of DOFMS needed to be worked out. Principal among these was the means of focusing ions at their respective flight distances at the time of detection. The theory of distance-of-flight focusing is reviewed in the next section. That task accomplished, Enke joined forces with the Hieftje and Koppenaal labs, which had an ongoing project (conducted with Bonner Denton at the University of Arizona) for the development of an ion array detector [termed the focal-plane camera (FPC)]; the FPC was then being applied with a magnetic-sector mass analyzer.

Partial funding for the construction of two identical proof-of-principle instruments was provided by the Pacific Northwest National Laboratory (see the Acknowledgments section). These instruments were constructed at Indiana University in the summer of 2009. Research on and development of these instruments followed in both labs. The experimental data presented in this article are largely the result of work done on the Indiana University instrument. The validity of the ion-focusing theory has been established, the simultaneous focus of ions at different flight distances has been verified, and the FPC has been successfully used in the DOFMS instrument.

2. ION FOCUSING IN DISTANCE-OF-FLIGHT AND TIME-OF-FLIGHT MASS SPECTROMETRY

Imagine a race in which the contestants are idly drifting about in the region of the starting line when the starting gun goes off. The situation is similar for both TOFMS and DOFMS when gaseous ion sources are employed. Given that not all the ions start from the same location and that they have various energies of motion in various directions at the time of acceleration, isobaric ions arrive at a time-of-flight detector over a range of times. This time spread gives rise to a finite peak width for each detected *m/z* value, with a consequent limitation on mass resolving power. Therefore, there are two variants (position and energy) among the initial ions whose effects need to be reduced to achieve good mass resolution. Reduction in the range of variation of these parameters can be achieved by filtering out all but a narrow band or by compensating for the variation to achieve focus for all ions. Of course, from the standpoint of sensitivity and throughput, focusing is superior to filtering. However, one cannot achieve both spatial and energetic focusing through any combination of static fields (4). Therefore, the current practice is to achieve focus for one variable and minimize the effect of the other.

2.1. Time-of-Flight Mass Spectrometry Focusing

In TOFMS instruments, the initial ion energy variations are minimized by use of a very strong acceleration field so that the effect of the initial energy of the ions in the flight path is small compared with their total energy. Further reductions in the initial energy dispersion are achieved by first forming a beam of ions, all moving at roughly the same velocity or energy, and then accelerating them orthogonally to the trajectory of the beam. Within the beam, lateral ion motion is minimized so that energy variations along the orthogonal axis of acceleration are reduced (5, 6).

When applied, the ion-extraction field is constant and persists until the last ion of interest has left the acceleration region. This method of ion extraction is termed constant-energy acceleration (CEA), as all ions accelerated over the same distance enter the field-free flight region with very nearly the same kinetic energy. Spatial dispersion, however, causes ions initially located further from the exit of the acceleration region to receive more energy by the time they exit than the ions that are closer to the exit. This energy disparity is exacerbated by the very high extraction field strength used to minimize the effects of the initial kinetic energy. Fortunately, as mentioned

above, the large energy variation caused by the spatial dispersion can be mostly overcome by the use of an ion mirror or reflectron. However, the mirror cannot be used to compensate the initial energy variation and the energy spread at the same time due to the spatial dispersion. Because the energy spread is larger, it is the spatial spread that gets compensated. Largely because of the uncompensated spread in initial energy, a limiting factor for mass resolution is created by ions that had rearward kinetic energy at the time of acceleration. The time required to reverse their motion before forward acceleration is termed the turnaround time. The later departure from the acceleration region of these so-called reverse ions cannot be compensated for by the ion mirror or by space focusing.

2.2. Distance-of-Flight Mass Spectrometry Focusing

The focusing requirements of DOFMS are very different from those of TOFMS. Instead of focusing ions of different *m/z* to the same flight distance, but at different times, all ions must be focused to *m/z*-dependent flight distances at the same time. The means for doing so are constant-momentum acceleration (CMA) and an ion mirror (7). When CMA is used, the motion of all the ions is increased in the direction of acceleration by the same momentum. CMA is achieved by terminating the acceleration pulse before any of the ions of interest leave the acceleration region. By this process, all the ions get the same "kick." The final momenta of ions with differing amounts of initial kinetic energy along the acceleration axis (forward or reverse) differ on that axis. Such differences in momenta among the ions are compensated for by differences in the time they spend in the ion mirror, so at a specific time, ions of equal *m/z* values return to their initial positions relative to one another. In this way, the initial energy dispersion is compensated for at the detection time, while the initial spatial dispersion remains the same as it was at the time of acceleration. Remarkably, this compensation for energetic variations includes the turnaround time. Thus, in DOFMS, the initial energy variations are compensated for (focused), and the initial spatial dispersion is retained—the exact complement to the situation in TOFMS. In contrast, turnaround time is not a limiting factor in DOFMS; rather, it is the spatial dispersion of ions in the direction of acceleration at the time of acceleration.

Figure 3 shows a SIMION® simulation of distance-of-flight focus of the initial ion beam (7). In this simulation, the geometry of the instrument is somewhat different from that in **Figure 1** in that the field-free flight path is divided into two parts, one before the mirror and one after. In this geometry, the detector is located in the section after the mirror. Distance of flight orthogonal to the initial ion-beam direction is shown as a function of time. The case of initial spatial dispersion is not shown. In DOFMS, this initial dispersion can be the limiting factor in mass resolution. Ion sources with minimal initial dispersion, such as surface desorption/ionization, would complement very well the energy-focus qualities of DOFMS. Because the spatial dispersion remains constant, the ratio of the ion-packet width to total flight distance declines (resolving power increases) if longer flight paths are used.

Figure 3 also shows that the penetration distance of ions into the mirror is *m/z* dependent. At constant momentum, ions with lower *m/z* values have a greater energy than do ions with higher *m/z* values. Therefore, the former travel further into the mirror field before turning around, which means that with CMA, ions turn around over a significant fraction of the mirror depth. Thus, mirrors used for DOFMS need to have a uniform field strength throughout a wide turnaround region, whereas with CEA and TOFMS, ions of all *m/z* values turn around in the same general region.

With CMA, the magnitude of the momentum impulse applied is the field strength of the acceleration pulse (E_p) times its duration (τ). Interestingly, within limits, the temporal shape

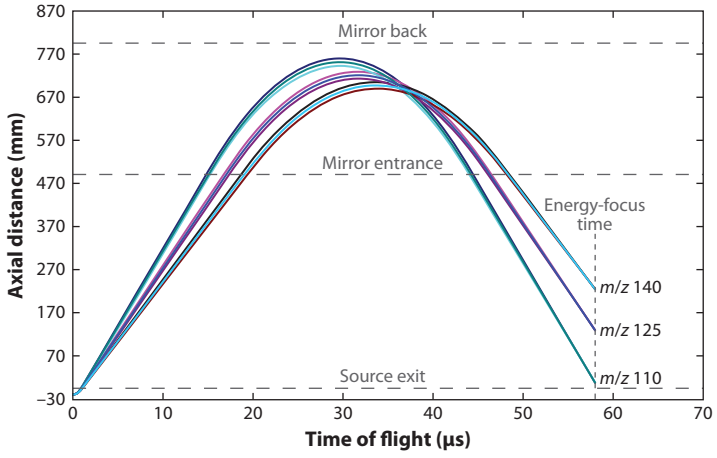

Figure 3

SIMION®-derived trajectories of singly charged ions with an atomic mass of 110, 125, or 140 in a hypothetical instrument with a field-free path of ~0.5 m before and after the mirror. For each *m/z* value, there are three ions; each has −0.2, 0.0, or +0.2 eV of initial kinetic energy in the direction of its acceleration. Part of the field-free flight path is before the mirror, and part after. Ions having the three different *m/z* values have different flight distances at the detection time of 57.27 μs. The differences in initial kinetic energy cause different velocities and divergent paths. Energy focus is achieved for all ions at the same detection time. Ions with lower *m/z* have greater energy and penetrate further into the mirror. Reproduced from Reference 7 with permission.

of the pulse is not important. The resulting ion velocity (neglecting the ions' initial energy) is proportional to $E_p\tau$ and is inversely proportional to *m/z*. **Figure 4** illustrates this inverse relationship between *m/z* and distance of flight. According to the relationship among flight distance, *m/z*, and resolution, it may make sense to use only the far part of the flight path for the array detector, splitting the field-free region before and after the mirror. The detectable ratio of high to low *m/z* depends on the relative lengths of the detector and the field-free flight path length. By cycling over only a few range settings, one can cover a relatively large *m/z* ratio range.

2.3. A Brief Review of Constant-Momentum Acceleration

Although investigators have long known about CMA (8), it has rarely been applied in analytical mass spectrometers. Poschenrieder (9) achieved energy focus for time-of-flight mass analyzers through a combination of CMA and magnetic sectors. Ioanoviciu has developed theoretical analyses of CMA used in TOFMS with hyperbolic electrode ion sources (10) and with an ion mirror in combination with delayed extraction (11). Most recently, Barovsky et al. (12) employed a nonlinear acceleration field with CMA for enhanced ion selection in TOFMS instrumentation. These examples demonstrate that the concept of CMA has intrigued investigators for some time, but its implementations have not yet been widely accepted in the instrumentation community. In conjunction with magnetic sectors (which operate on differences in ion momenta), the sector could serve as a focusing device rather than as a dispersive device. CMA in conjunction with TOFMS does not provide *m/z*-independent focusing at the time-of-flight detector (7). However, CMA is perfectly suited to DOFMS focusing in that it provides *m/z*-independent focusing at all distances of flight at the same time.

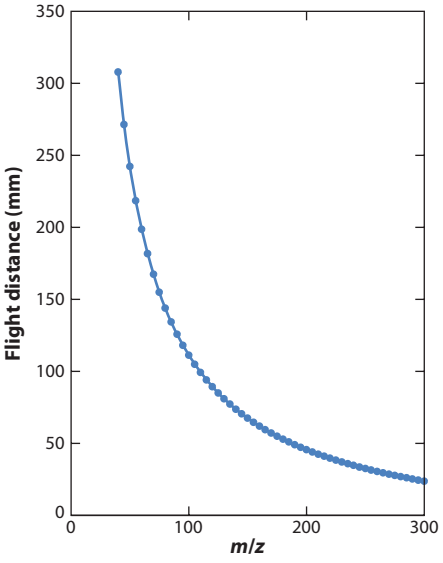

Figure 4

Ions with an *m/z* of 40 are set to focus at the longest flight distance of 310 mm. Ions with an *m/z* of 250 are then focused at a flight distance of 40 mm. Because of the reciprocal relationship between *m/z* and flight distance, the separation in flight distance between adjacent unit *m/z* values drops as *m/z* increases. (The dots occur every 5 *m/z*.) If the detector is placed over the most distant half of the field-free flight path, the ratio of high *m/z* to low *m/z* detected is two, and the resolution ratio from one end of the detector to the other is four.

2.4. The Mathematics of Distance-of-Flight Mass Spectrometry Focusing

At the end of the CMA pulse, the momentum of the ions (mass times velocity), mv_p, is

$$mv_p = mv_{\text{imp}} + mv_o = zq_e E_p \tau + mv_o, \tag{1}$$

where v_{imp} is the velocity gained by the CMA pulse, zq_e is the nominal charge on the ion times the absolute value of the charge on an electron, $E_p \tau$ is the CMA pulse field strength multiplied by the pulse duration, and mv_o is the initial momentum of the ions in the direction of the acceleration. This equation reveals two important facts about the momentum received by the ions from the CMA pulse: (*a*) It is proportional to the charge, so momentum is a constant only for ions of the same charge, and (*b*) the momentum depends on the product of the field strength and time, which is the area under the pulse profile, so the pulse can be any shape so long as it is reproducible and terminates before any ion of interest leaves the source.

The time the ions spend in the source and the field-free region can be derived from the velocity v_p in Equation 1. The time in the source t_s depends on the initial location of the ions at the time of acceleration ($s_o + \Delta s_o$) and on the initial ion velocity and direction (Equation 2):

$$t_s = \frac{s_o + \Delta s_o}{\frac{zq_e E_p \tau}{m} + v_o} + \frac{\tau}{2}\left(\frac{1}{1 + \frac{mv_o}{zq_e E_p \tau}}\right). \tag{2}$$

The time the ions spend in the mirror, t_M, which has a constant field strength, is

$$t_M = \frac{2mv_p}{zq_e E_M}, \tag{3}$$

where E_M is the field strength in the mirror. Equation 3 reveals that the mirror time is proportional to the momentum; therefore, it is approximately the same for all ions of the same charge but differs by an amount that depends on the initial ion velocity and direction.

Now the distance the ions travel in the field-free region L_{FF} up to the time of detection t_{det} can be calculated:

$$L_{FF} = v_p\,(t_{det} - t_M - t_s)\,. \tag{4}$$

After substitution in Equations 1 through 3 and rearrangement, the flight distance at the time of detection is determined to be

$$L_{FF} = v_{imp}t_{det} - \frac{2mv_{imp}^2}{zq_eE_M} - (s_o + \Delta s_o) - \frac{\tau\, v_{imp}}{2} + v_o t_{det} - \frac{4mv_{imp}v_o}{zq_eE_M} - \frac{2mv_o^2}{zq_eE_M}. \tag{5}$$

The last three terms in Equation 5 are the variations in the distance traveled as a result of the initial ion velocity; of these, the last term is the least significant. The second and third terms from the end of Equation 5 can cancel through an appropriate choice of t_{det}. This detection time, t_{ef}, is termed the energy-focus time:

$$t_{ef} = \frac{4mv_{imp}}{zq_eE_M} = \frac{4\tau E_p}{E_M}. \tag{6}$$

Substituting t_{ef} for t_{det} in Equation 5 yields our final equation for the flight distance at $t_{ef}[L_{FF(t_{ef})}]$, where U_o is the initial ion energy:

$$L_{FF(t_{ef})} = \frac{zq_eE_p\tau}{m}\left(\frac{2L_M\tau}{E_M} - \frac{\tau}{2}\right) - (s_o + \Delta s_o) - \frac{4\,|U_o|}{zq_eE_M}. \tag{7}$$

Equation 7 shows that the flight distance is inversely proportional to the ion *m/z*, that the initial spatial dispersion remains unchanged in the packet width at the time of detection, and that there is a second-order effect of the initial energy dispersion that is not focused. This term can be minimized by the use of greater CMA pulse fields and the longest practical pulse time.

2.4.1. Multicharged ions. A very interesting aspect of DOFMS is the effect of the ionic charge state. As mentioned above, the momentum gained by the ion from the CMA pulse is proportional to the ionic charge. Considering the velocities of ions of the same mass but different charges, such as those generated in electrospray ionization (ESI), we see that the velocities and therefore the distance traveled by isomass ions in a given time are proportional to their charge. In other words, the ions are linearly placed along the flight axis (**Figure 5**).

The flight distance difference between ions of adjacent charge number is

$$\Delta L_{FF,\Delta z=1} = \frac{q_eE_p\tau}{m}\left(\frac{2L_M\tau}{E_M} - \frac{\tau}{2}\right). \tag{8}$$

All of the terms in Equation 8 are known, which means that the ions' *m/z* can be determined by the flight distance, and their mass can be calculated from the flight distance between consecutive charge values. An algorithm could be developed to find the responses that occur at equally spaced intervals to produce a calculated singly charged mass spectrum, as is done with conventional ESI today. Because of the equal spacing of distances between consecutive charge values, the algorithm for detection and assignment of charge state will be different and potentially simpler.

2.4.2. Physical constraints. To develop a practical DOFMS instrument, several constraints must be invoked. First, the ions with the lowest *m/z* of interest must not leave the acceleration region before the acceleration pulse has ended. Second, the voltage in the last element of the ion mirror must be larger than the kinetic energy in electronvolts of the lowest *m/z* ion of interest. Third, the

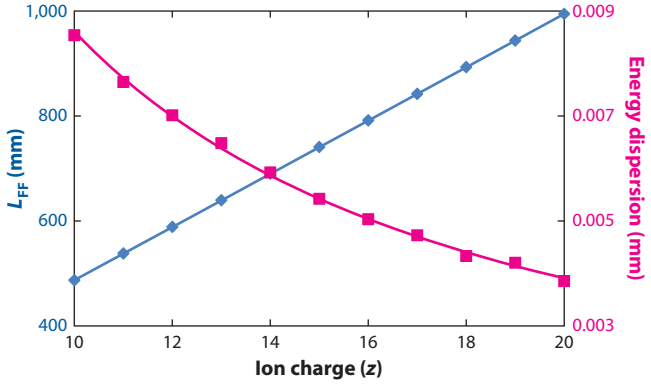

Figure 5

Flight distance as a function of z for ions of $m = 15{,}000$ Da. A 1-m field-free flight path was presumed in these simulated results. The linear relation between the flight distance at the energy-focus time and the charge number is shown. The magenta line with the right axis is the uncompensated initial energy of these ions for an initial energy dispersion of ± 0.2 eV. Abbreviation: L_{FF}, flight distance at the time of detection. Reproduced from Reference 7 with permission.

mirror depth must be a little more than one-fourth of the field-free flight distance of the lowest m/z ion to be detected at the detection time (the field-free distance to the furthest detector element). Finally, the ratio of the highest to lowest m/z–valued ions to be detected by the detector array depends on the fraction of the total field-free flight path that the detector occupies. Equation 9 gives this m/z range ratio:

$$\frac{(m/z)_{high}}{(m/z)_{low}} = \frac{(L_{FF})_{far}}{(L_{FF})_{near}} = \frac{1}{1 - L_D/(L_{FF})_{far}}. \quad (9)$$

Here $(L_{FF})_{near}$ is the flight distance to the first encountered element in the detector; $(L_{FF})_{far}$ is the distance to the last; and L_D, the difference between them, is the length of the detector. If the field-free region is equally split before and after the mirror and the detector occupies the total space after the mirror, the ratio of high- to low-m/z values observed is two. For the more typical 4:1 m/z ratio, one-fourth of the field-free region can precede the ion mirror. If the extraction region abuts the entrance to the ion mirror, the achievable m/z ratio approaches infinity. These constraints are employed in the design of and results from the proof-of-principle instrument described in the next section.

3. A PROOF-OF-PRINCIPLE DISTANCE-OF-FLIGHT MASS SPECTROMETRY INSTRUMENT

Figure 6 depicts the interior parts of the DOFMS instruments in operation at the Hieftje lab at Indiana University and at the Koppenaal lab at the Pacific Northwest National Laboratory (13). In this type of instrument, a metallic sample is ionized by a glow discharge. The ions produced are formed into a beam that is focused in the CMA extraction region. The 31.25-cm total field-free region is split into two sections, one before and one after the ion mirror (linear-field reflectron). All voltages and pulse timings are set under computer control. The orthogonal deflection of the beam toward the detector system uses CEA. This method has the advantage of focusing ions that have different distances from the detector at a plane parallel to the axis of the beam. This plane is termed the space-focus plane, and it is located at twice the distance from the acceleration region

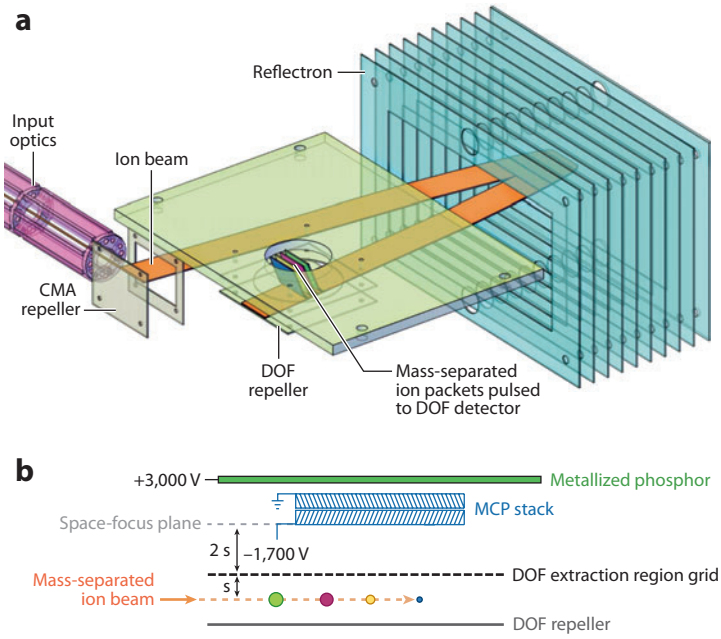

Figure 6

(*a*) Illustration of a distance-of-flight (DOF) instrument internal parts with the ion beam highlighted in orange. A section of the input ion beam is pulsed into the flight path by constant-momentum acceleration (CMA). Following turnaround in a linear-field reflectron, ions at all distances are focused at the energy-focus time t_{ef}. Slightly before t_{ef}, a constant-energy acceleration (CEA) pulse pushes the *m/z*-separated ions upward onto a spatially selective ion detector (not shown). (*b*) Side view of the DOF extraction region. The microchannel plate (MCP)-phosphor detection assembly is at a position of 2 s from the CEA region. Reproduced from Reference 13 with permission.

as the average ion distance from the acceleration region exit (14). Of course, it takes some time for the ions to transit from the beam to the detector surface; optimal resolution is obtained if the ions are detected at time t_{ef}. Therefore, the CEA pulse that drives the ions to the detector is applied at a time slightly before t_{ef}.

3.1. Results with a Microchannel Plate–Phosphor Detector System

The first detector system with which this instrument was fit was chosen for its simplicity of installation. It is a dual microchannel plate (MCP) that operates as a conversion dynode (which converts ion energy to electron emission) at its entrance and an electron multiplier. Because an image of the ion impacts on the MCP is desired, the amplified electrons impinge on a phosphor plate to produce a light image that can be seen through a transparent port. **Figure 6*b*** shows the MCP-phosphor detector and the detection-time deflection scheme (13).

The ion packets appear as light bands on the phosphor; each band is parallel to the plane of the CMA repeller. These bands were observed through a transparent port in the instrument cover and were photographed through this same port to provide a record of the spectrum. **Figure 7** presents an example of such photographs (13).

Subsequent to taking the photograph, the images were scanned to provide a plot of image intensity versus either distance or calculated *m/z*. **Figure 8** shows a typical *m/z* spectrum (13).

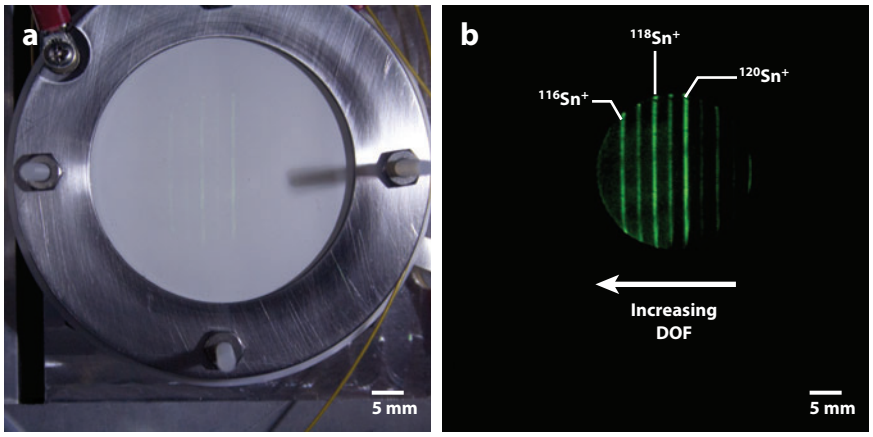

Figure 7

Photographs taken with a digital camera of microchannel plate–phosphor assembly illuminated (*a*) with white light and (*b*) without background light. The images were captured through a Plexiglas® viewport directly above the distance-of-flight (DOF) detection region. (*b*) The DOF mass spectrometric lines represent the isotopes of Sn from glow discharge of a bronze sample. Reproduced from Reference 13 with permission.

The scanned image was taken with an intensified charge-coupled device camera that has a linear response function. Any particular *m/z*-value ions can be placed within the detector area; the range of *m/z* values observable at any one time is given by Equation 9. In this case, if the total flight path is 31.25 cm and the usable portion of the detector is 2.5 cm, the ratio of high- to low-*m/z* ions observable is 1.08, exactly as shown in this spectrum.

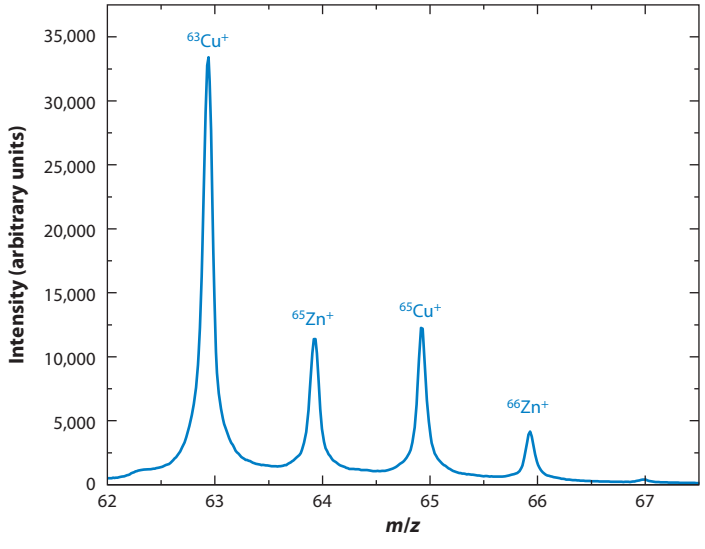

Figure 8

Distance-of-flight mass spectrometry mass spectrum resulting from photographing the detection phosphor. The *m/z* range is limited by the 25-mm detector diameter. Other, similar spectra, shown in Reference 13, are for Cr, Sn, and Pb and demonstrate the ability to place any portion of the spectrum in the distance range of this detector. The *m/z* resolving power of the spectra over the entire elemental range is 400.

Although the MCP-phosphor camera has provided the results predicted by theory and simulation, it has some significant limitations for this application, including restricted dynamic range, nonlinearity of response, and limited resolution. The chevron arrangement of the two MCPs used and the space between the MCP and the phosphor contribute to the spreading of electrons beyond the relatively small pitch of the capillaries in the MCP (15). Having served its purpose, the MCP-phosphor detection system has been replaced by a solid-state FPC. The characteristics of this camera and the results of its installation in the DOFMS instrument are described in the next section.

3.2. Results with the Focal-Plane Camera Detection System

An FPC is a linear array of Faraday strips with associated charge-integrating and readout electronics. It was originally designed to operate on the focal plane of a Mattauch-Herzog mass spectrograph (16). The FPC-512 is the third in a series of increasingly sophisticated detector arrays built for simultaneous, wide-spectrum mass-spectral detection (17–21), but it serves very well in the DOFMS instrument, demonstrating the superior performance of this type of detector and the practicality of using such detectors in commercial DOFMS systems. The 512 detector strips make a detector array that is only 6.4 mm long. Each of the 8.5-μm-wide strips has a dedicated integrating amplifier with two levels of gain that can be computer programmed to be in either state. The detector strips respond to the charge (not the energy) of the ions that strike it, which leads to detection with no mass bias or mass limit. The limit of detection is roughly 100 charges. The output signals from the array of integrating amplifiers are serially read out to an analog-to-digital converter for computer interpretation into a mass spectrum. The controllable dynamic range is greater than 10^8, which demonstrates that the dynamic range of an array with programmable gain array elements exceeds that attainable with time-of-flight systems when acquiring full spectra. Modern semiconductor fabrication techniques were used in the FPC's construction, so it is amenable to large-scale production.

The FPC-512 has been installed in the proof-of-principle instrument described above (2). The very short length of the detector array in the FPC-512 severely limits the m/z range that can be detected on each ion extraction. Equation 9 shows that the ratio of high to low m/z falling on the detector for any given extraction is only 1.023. In this prototype instrument, one can view 4.6 Da in the region of Pb, 2.6 Da for Sn isotopes, and 1.4 Da in the Cu and Zn region. Although this is too small for most practical applications, it demonstrates the advantages of using this type of detector with DOFMS. A larger m/z ratio can be obtained by decreasing the length of the field-free region or increasing the dimensions of the detector. The technology used in the FPC-512 can be readily scaled up to a much larger array. A similar detector, 12 cm in length and with 4,800 dual-gain channels, has recently been introduced (see **http://www.spectro.com**). Because this dimension was achieved by stitching smaller sections together, even larger arrays can be achieved.

Because of the small fraction of the field-free region covered by the FPC-512 detector, a broader spectral range must be obtained by moving the m/z values impinging on the detector window in a series of extractions. Per Equation 7, the m/z value for any specific L_{FF} at the energy-focus time can be set by varying $E_p\tau$ or E_M. Because $E_p\tau$ is set to meet the requirements of CMA, it is simplest to adjust E_M. Equation 6 shows that the energy-focus time is a function of E_M, so the detect time must be adjusted as well. These equations can be used to calculate the required values in advance so that the range changes can be done quickly and accurately.

The spectrum in **Figure 2** (2) was obtained with the FPC-512. All of the Pb isotopes were focused onto the FPC. The large number of elements in the array enabled an accurate measurement of packet length (~350 μm) and peak shape (Gaussian). To obtain a spectrum of the Cu and Zn

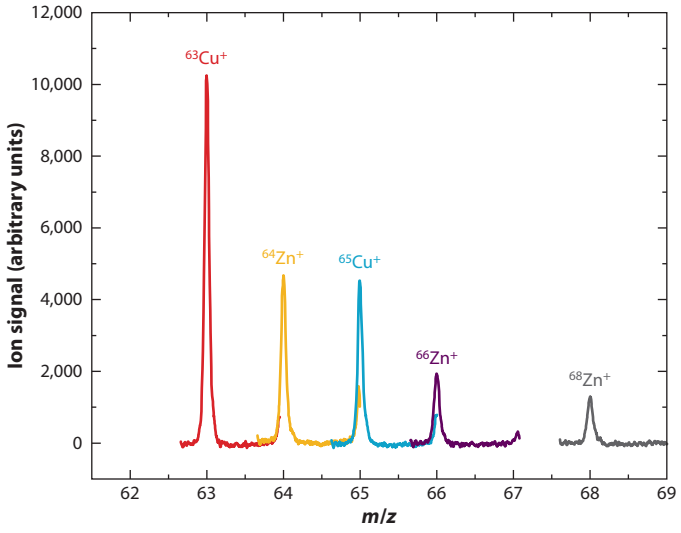

Figure 9

In this *m/z* region, the *m/z* window is 1.4 Da. Five independent spectra are combined in this composite spectrum. Ions of all *m/z* values remain in focus when only the mirror voltage and the detection time are changed to alter the *m/z* range detected. The mass resolution is between 700 and 800. Reproduced from Reference 2 with permission.

isotopic pattern, it was necessary to acquire several spectra across the region from *m/z* 63 to 68. The spectrum shown in **Figure 9** is a composite of five individual spectra. It very closely illustrates the spectrum one would obtain if one had an array detector that was 31.5 mm long. As mentioned before, wider *m/z* ranges can be obtained with detectors that are a longer fraction of the length of the field-free flight distance of the lowest *m/z* of interest. However, **Figure 9** demonstrates that successive *m/z* windows can be acquired and assembled to extend the *m/z* range to whatever is desired. The achieved resolution is much higher with the FPC than with the MCP-phosphor detector, largely because of the elimination of image spread in the MCP.

4. FUTURE APPLICATIONS OF DISTANCE-OF-FLIGHT MASS SPECTROMETRY, INCLUDING SCANLESS TANDEM MASS SPECTROMETRY

It seems inevitable that the merits of adopting DOFMS for analytical mass spectrometry depend on its unique qualities, particularly in relation to those of TOFMS, with which it shares many characteristics. This is true because at its inception DOFMS would have to outperform mass analyzers that are already in their third (or higher) generation of development in basic specifications such as mass resolution, sensitivity, and adaptability to various ion sources. In this section, we consider DOFMS's qualities and the applications for which it is uniquely suited and where it may offer compelling advantages.

4.1. Where Array Detection Can Improve Performance

The merits of array detection over having all of the analytical information pass through a single-detector system stem from the fact that each detector in an array operates independently with

respect to its channel of information. With the single-detector system, there is always some data-rate limitation that constrains the dynamic range detectable in the same spectrum. The distribution of signal information among the many detectors in an array alleviates this problem. The use of autoranging electronics in each element of the array ensures a very large dynamic range of detectable ion fluxes. The disadvantage of array detection arises from the inevitable quantization along the *m/z* axis and a corresponding potential limitation in resolution. In addition, there are the usual trade-offs among detector length, field-free length, and *m/z* range and among field-free length, detector element pitch, and *m/z* resolution.

In mass spectrometry, the use of array detection relies on producing a difference in the physical paths through the instrument taken by ions of different *m/z* values. The only mass analyzer other than the DOFMS instrument that achieves this goal is the magnetic sector, or the Mattauch-Herzog geometry double-focusing mass analyzer. Indeed, array-detector systems for such mass analyzers have been developed and even commercialized. JEOL, Ltd., offered an array detector for its double-focusing systems for many years. Having multiple Faraday-type detectors in an array is standard among high-end isotope-ratio mass spectrometers, notably because of their need for wide dynamic range and extreme precision in abundance ratio measurement. Most recently, SPECTRO has developed an inductively coupled plasma Mattauch-Herzog mass spectrometer with a 4,800-element array detector for simultaneous detection over the entire elemental range (see **http://www.spectro.com**). In this application, a DOFMS analyzer is structurally simpler than a Mattauch-Herzog analyzer.

That each element of an array detector is an independent entity, devoted to its own range of *m/z* values, is especially important where a wide range of ion abundances is encountered. An example is survey analyses in which mass analysis follows chromatographic separation. In complex mixtures, it is common for high-abundance components to coelute with other components whose abundance may be four or more orders of magnitude lower (22). As these components generally fall on different detectors, each with its own autoranging electronics, huge abundance disparities can be easily accommodated. Current time-of-flight mass analyzers do have a tremendous dynamic range, but the extremes of this range are achieved by an adjustment of the integration time for each spectrum acquired. When the instrument is operated as a chromatographic detector, the integration time (which is the inverse of the spectrum-collection rate) must remain constant. Here is where high ion throughput, in combination with the very wide dynamic range of an array detector, might offer a distinct advantage in revealing components at even lower levels of abundance than are currently detected.

The elements of an ion detector array can be simple Faraday charge collectors. Such detectors have two distinct advantages if the minimum detectable charge can be made small enough. One advantage is perfect quantitation in that the charge response per ion hitting the surface is the ion charge, *qz*. The sum of the collected charges must be an exact linear function of the number of ions impinging the surface since the previous readout. The second, corollary advantage is that there is no upper mass drop-off in sensitivity or, indeed, any upper limit to the *m/z* of the ions that can be detected.

4.2. Where Energy Focusing Is Advantageous

A unique quality of DOFMS is the spatial focus of ions of disparate initial kinetic energies. Such initial-energy dispersions are encountered with gaseous ion sources, especially when they are thermally hot, such as with glow-discharge or inductively coupled plasma sources. In addition, ions extracted from gaseous sources have initial velocities toward and away from the acceleration region exit, which results in the deleterious turnaround delay. Many surface ionization sources

such as matrix-assisted laser desorption/ionization, although not plagued by the turnaround effect, do produce ions with a very broad kinetic energy dispersion. For such sources, the energy-focusing capability of DOFMS may be a distinct advantage.

4.3. Where Collection of Ions Physically Separated by *m/z* Is Sought

As mentioned above, DOFMS and the magnetic sector are the only two *m/z* analyzers that produce differences in ion paths by which ions of different *m/z* are registered by different physical detectors. This characteristic creates the potential for the ions impinging on the detector array to be selectively harvested. Thus, the array detector could be replaced by a series of soft-landing sites (23–27) for efficient ion collection and release. This arrangement would enable the collection of individual isotopes of atoms or compounds, different mass forms of biomolecules, and physical separation of very large biostructures. The great advantage of DOFMS over currently used *m/z*-selective ion collectors is that with DOFMS one can collect ions of all of the detectable *m/z* values simultaneously with virtually no upper mass limit, rather than sequentially.

4.4. Where Truly Unlimited *m/z* Range Is Needed

Mass spectrometry has made tremendous strides in recent years with respect to the *m/z* of molecules that can be *m/z* separated and detected. Still, there is an upper limit to the ion mass that can be recorded by traditional detectors. Such detectors require some sort of conversion of the detected ion energy into the release of one or more electrons that can then be amplified by electron multiplication into a detectable signal. The efficiency of the ion energy–to–electron release device falls off dramatically as the ion mass increases (28). Methods of extending the detectable mass range include postseparation acceleration (29), postseparation dissociation into smaller–mass fragment ions (30), and cryogenic detection (31). Even with these extensions, there is a strong interest in mass spectrometry of still higher mass entities (28) that can currently be satisfied only by special types of mass analysis such as the charge-induction tube (32) and specially modified quadrupole ion traps (33, 34). DOFMS provides a unique method for mass analysis in this very high mass region. Here, the magnetic-sector combination with array detection is not a viable alternative, given the inherent limitation of the magnetic sector for high-*m/z* separation (28).

4.5. Where Scanless, Simultaneous Tandem Mass Spectrometry Is Desired

Tandem mass spectrometry (MS/MS) can potentially produce a three-dimensional data space of selected *m/z*, fragmentation-product *m/z*, and intensity. For mixtures ionized by soft methods, this data space would provide the product spectrum of all of the mixture components. For single species ionized by fragmenting ionization, this data space would provide all of the product spectra of all of the ions in the initial mass spectrum. In MS/MS terms, this is all the information that can be obtained from a simple mass spectrum, all the product-scan spectra, all the precursor-scan spectra, and all the neutral-loss spectra. Collection of all this information from a single sample, however valuable it might be, is rarely done. The most efficient way to do so with current technology would be to use an MS/MS instrument in which the product *m/z* is obtained by TOFMS and a product spectrum is collected for every *m/z* value in the precursor spectrum. This approach simply takes more time and sample than are generally available. The concept of an instrument that can disperse both precursor *m/z* and product *m/z* onto a two-dimensional detector has been a vision of instrumentalists ever since the early days of MS/MS (35). In the Zare lab, a combination of its Hadamard TOFMS instrument with ion fragmentation in the ion mirror (by postsource decay

or surface-induced dissociation) and an imaging ion–arrival time detector has demonstrated the separate detection of product ions and the potential for MS/MS operation (36). Another approach, involving modulated ion excitation in a Fourier transform ion cyclotron mass spectrometer, was first proposed in 1987 (37) and has been further developed in several stages since then (38).

One way to collect all of the product-*m/z* information from all of the precursors at once is to fragment all of the precursor ions in a way such that the product ions retain information about their precursor *m/z*. When ions fragment spontaneously, the product ions retain the same velocity as their precursor ions (plus or minus the energy of fragmentation). Thus, the distance over which the product ions fly in a specific amount of time is related to their precursor *m/z*. A position-sensitive time-of-flight analyzer can then determine the product mass at each precursor

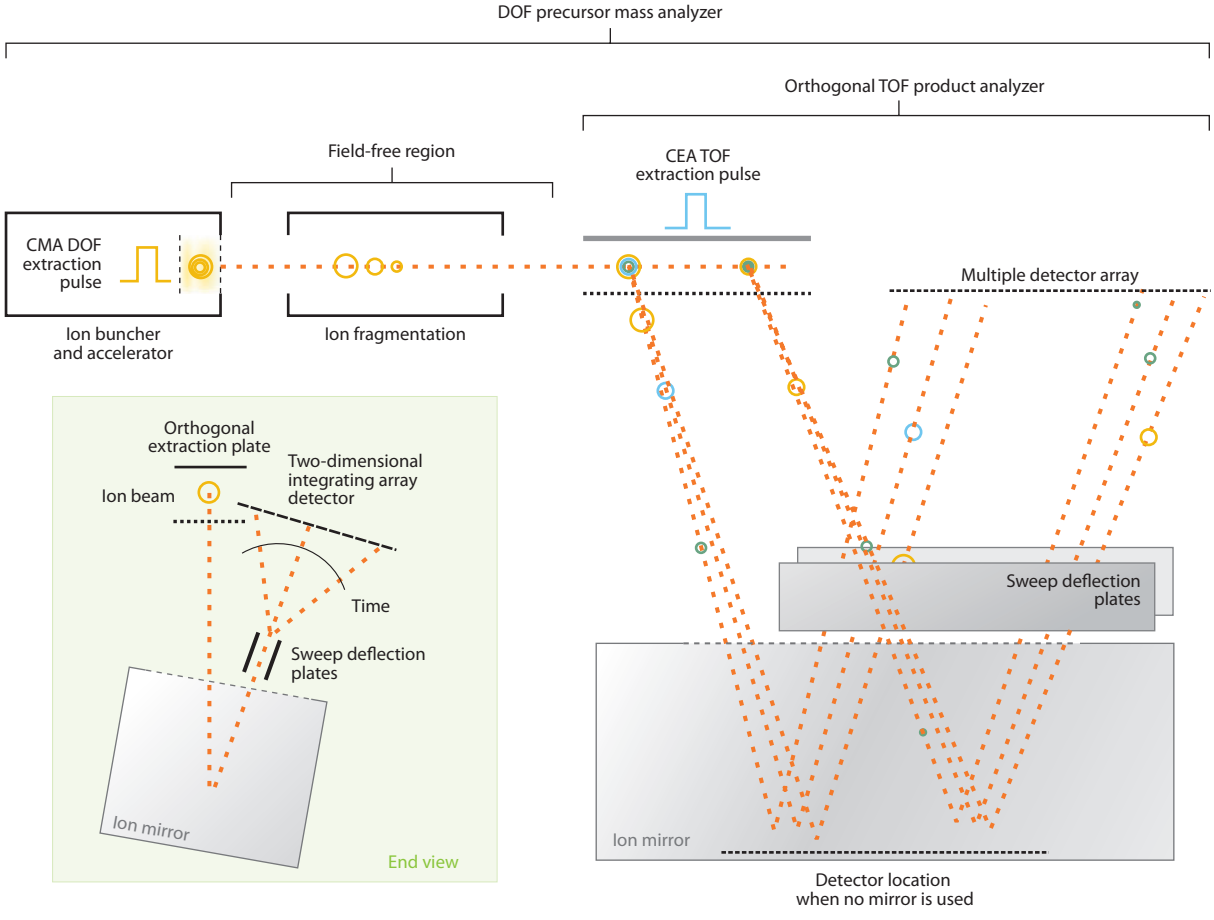

Figure 10

Simultaneous tandem mass spectrometry can be accomplished by a combination of distance-of-flight (DOF) and time-of-flight (TOF) mass spectrometry. The precursor ions are accelerated out of the source in a batch, fragmented by nonscattering fragmentation, and orthogonally accelerated into a position-sensitive TOF analyzer. The flight time in the TOF analyzer gives the product *m/z*, and the position of its detection is related to the precursor *m/z*. Constant-momentum acceleration (CMA) is used to accelerate the initial ion batch. The ion mirror required to provide precursor-*m/z* focus is omitted for simplicity. The TOF detector can be an array of arrival-time detectors, or a two-dimensional detector array can be used with a scanning method (*inset*). Abbreviation: CEA, constant-energy acceleration. Reproduced from Reference 39.

position (**Figure 10**). This instrument concept was first proposed in 2003 (3, 39) but has not yet been implemented. The first requirement for its implementation is the method of achieving DOFMS focusing, which is now being demonstrated in the DOFMS instruments described above. The second requirement is an efficient method for instantaneous fragmentation, such as UV photodissociation or electron-capture dissociation. The third requirement is that of the time-sensitive detector array, which could be of the sort of detection systems now used in TOFMS or, with the deflection system suggested in **Figure 10**, a three-dimensional ion detector array. Thus, DOFMS, in combination with TOFMS, offers a way to realize simultaneous MS/MS in real time with an unlimited *m/z* range, a high dynamic range, and physical separation of all of the product ions.

DISCLOSURE STATEMENT

The authors are not aware of any affiliations, memberships, funding, or financial holdings that might be perceived as affecting the objectivity of this review.

ACKNOWLEDGMENTS

Our work is supported in part by the National Science Foundation through grant DBI-1062846, the U.S. Department of Energy through grant DE-FG02-98ER14890, by the Lilly Endowment–Indiana MetaCyt Initiative, and by Laboratory Directed Research and Development funds from Pacific Northwest National Laboratory (operated by Battelle Memorial Institute under contract to the U.S. Department of Energy).

LITERATURE CITED

1. Cassiday L. 2007. Distance of flight: a new paradigm for MS. *Anal. Chem.* 79:8830
2. Graham AW, Ray SJ, Enke CG, Felton JA, Barinaga CJ, et al. 2011. Resolution and mass range performance in distance-of-flight mass spectrometry with a multichannel focal-plane camera detector. *Anal. Chem.* 83:8552–59
3. Enke CG. 2006. Distance of flight spectrometer for MS and simultaneous scanless MS/MS. *US Patent 7,041,968*
4. Yefchak GE, Enke CG, Holland JF. 1989. Models for mass-independent space and energy focusing in time-of-flight mass spectrometry. *Int. J. Mass Spectrom. Ion Process.* 87:313–30
5. Dawson JHJ, Guilhaus M. 1989. Orthogonal-acceleration time-of-flight mass spectrometer. *Rapid Commun. Mass Spectrom.* 3:155–59
6. Dodonov AF, Chernushevich IV, Laiko VV. 1991. Atmospheric pressure ionization time-of-flight mass spectrometer. In *Book of Abstracts of the Twelfth International Mass Spectrometry Conference*, p. 153
7. Enke CG, Dobson GS. 2007. Achievement of energy focus for distance-of-flight mass spectrometry with constant momentum acceleration and an ion mirror. *Anal. Chem.* 79:8650–61
8. Wolff MM, Stephens WE. 1953. Pulsed mass spectrometer with time dispersion. *Rev. Sci. Instrum.* 24:616–17
9. Poschenrieder WP. 1971. Multiple-focusing time of flight mass spectrometers. Part I. TOFMS with equal momentum acceleration. *Int. J. Mass Spectrom. Ion Phys.* 6:413–26
10. Ioanoviciu D. 1998. Perfect velocity focusing in hyperbolic electrode source-drift space time-of-flight mass analyzers. *Rapid Commun. Mass Spectrom.* 12:1925–27
11. Ioanoviciu D. 1999. Delayed extraction-constant momentum time-of-flight mass spectrometry. *Nucl. Instrum. Methods A* 427:157–60
12. Barofsky DF, Piyadasa G, Hakansson P. 2004. Mass spectrometer. *World Intellect. Patent Organ. Appl. PCT/US2003/027298*
13. Graham AW, Ray SJ, Enke CG, Barinaga CJ, Koppenaal DW, Hieftje GM. 2011. First distance-of-flight instrument: opening a new paradigm in mass spectrometry. *J. Am. Soc. Mass Spectrom.* 22:110–17

14. Cotter RJ. 1997. *Time-of-Flight Mass Spectrometry*. Washington, DC: Am. Chem. Soc.
15. Birkenshaw K. 1997. Fundamentals of focal plane detectors. *J. Mass Spectrom.* 32:795–806
16. Knight AK, Sperline R, Hieftje GM, Young ET, Barinaga CJ, et al. 2002. The development of a micro-Faraday array for ion detection. *Int. J. Mass Spectrom. Ion Phys.* 215:131–39
17. Barnes JHIV, Sperline R, Denton MB, Barinaga CJ, Koppenaal D, et al. 2002. Characterization of a focal plane camera fitted to a Mattauch-Herzog geometry mass spectrograph. 1. Use with a glow-discharge source. *Anal. Chem.* 74:5327–32
18. Barnes JH, Schilling GD, Sperline R, Denton MB, Young ET, et al. 2004. Characterization of a focal plane camera fitted to a Mattauch-Herzog geometry mass spectrograph. 2. Use with an inductively coupled plasma. *Anal. Chem.* 76:2531–36
19. Schilling GD, Andrade FJ, Barnes JH, Sperline RP, Denton MB, et al. 2006. Characterization of a second-generation focal-plane camera coupled to an inductively coupled plasma Mattauch-Herzog geometry mass spectrograph. *Anal. Chem.* 78:4319–25
20. Schilling GD, Ray SJ, Rubinshtein AA, Felton JA, Sperline RP, et al. 2009. Evaluation of a 512-channel Faraday–strip array detector coupled to an inductively coupled plasma Mattauch-Herzog mass spectrograph. *Anal. Chem.* 81:5467–73
21. Felton JA, Schilling GD, Ray SJ, Sperline RP, Denton MB, et al. 2011. Evaluation of a fourth-generation focal plane camera for use in plasma-source mass spectrometry. *J. Anal. At. Spectrom.* 26:300–4
22. Enke CG, Nagels LJ. 2011. Undetected components in natural mixtures: how many? What concentrations? Do they account for chemical noise? What is needed to detect them? *Anal. Chem.* 83:2539–46
23. Franchetti V, Solka BH, Baitinger WE, Amy JW, Cooks RG. 1977. Soft landing of ions as a means of surface modification. *Int. J. Mass Spectrom. Ion Phys.* 23:29–35
24. Grill V, Shen J, Evans C, Cooks RG. 2001. Collisions of ions with surfaces at chemically relevant energies: instrumentation and phenomena. *Rev. Sci. Instrum.* 72:3149–79
25. Laurens CR, Venema L, Kemerink GJ, Niesen L. 1997. Soft-landing deposition of mass-separated radioactive isotopes. *Nucl. Instrum. Methods B* 129:429–35
26. Miller SA, Luo H, Pachuta SJ, Cooks RG. 1997. Soft-landing of polyatomic ions at fluorinated self-assembled monolayer surfaces. *Science* 275:1447–50
27. Ouyang Z, Takats Z, Blake TA, Gologan B, Guymon AJ, et al. 2003. Preparing protein microarrays by soft-landing of mass-selected ions. *Science* 301:1351–54
28. Chang H-C. 2009. Ultrahigh-mass mass spectrometry of single biomolecules and bioparticles. *Annu. Rev. Anal. Chem.* 2:169–85
29. Gilmore IS, Seah MP. 2000. Ion detection efficiency in SIMS: dependencies on energy, mass and composition for microchannel plates used in mass spectrometry. *Int. J. Mass Spectrom.* 202:217–29
30. Coval X. *HM2 and HM2 TUVO: next generation of high-mass MALDI retrofit systems*. Zürich: CovalX. **http://www.covalx.com/files/HM2_High-Mass_Systems.pdf**
31. Wenzel RJ, Matter U, Schultheis L, Zenobi R. 2005. Analysis of megadalton ions using cryodetection MALDI time-of-flight mass spectrometry. *Anal. Chem.* 77:4329–37
32. Fuerstenau SD, Benner WH, Thomas JJ, Brugidou C, Bothner B, Siuzdak G. 2001. Mass spectrometry of an intact virus. *Angew. Chem. Int. Ed.* 40:541–44
33. Nie Z, Tzeng Y-K, Chang H-C, Chiu C-C, Chang C-Y, et al. 2006. Microscopy-based mass measurement of a single whole virus in a cylindrical ion trap. *Angew. Chem. Int. Ed.* 45:8131–34
34. Nie Z, Cui F, Tzeng Y-K, Chang H-C, Chu M, et al. 2007. High-speed mass analysis of whole erythrocytes by charge-detection quadrupole ion trap mass spectrometry. *Anal. Chem.* 79:7401–7
35. McLafferty FW, ed. 1983. *Tandem Mass Spectrometry*. New York: Wiley
36. Yoon OK, Robbins MD, Zuleta IA, Barbula GK, Zare RN. 2008. Continuous time-of-flight ion imaging: application to fragmentation. *Anal. Chem.* 80:8299–307
37. van der Rest G, Marshall AG. 2001. Noise analysis for two-dimensional tandem FT-ICR mass spectrometry. *Int. J. Mass Spectrom.* 208:101–11
38. Pfändler P, Bodenhausen G, Rapin J, Houriet R, Gäumann T. 1987. 2D FT/ICR/MS. *Chem. Phys. Lett.* 138:195–200
39. Enke CG. 2003. *Simultaneous MS/MS—all the products of all the precursors all the time.* Presented at Am. Soc. Mass Spectrom. (ASMS) 2003, Montreal, Can.

Annual Review of
Analytical Chemistry

Volume 5, 2012

Contents